ECB

# CRYSTAL STRUCTURE, VISUALIZATION, ESR, THERMAL, AND SPECTRAL STUDIES AND MICROSTRUCTURAL FEATURES OF THORIUM-DOPED $Pb_{1-x}Th_xZrO_3$ PEROVSKITE

**Khaled M.Elsabawy**[a,b]

**Keywords:** Crystal Structure; Thorium-doped lead zirconate; Doping; Perovskite

The pure lead zirconate ($PbZrO_3$) and low concentrations thorium-doped samples with general formula ($Pb_{1-x}Th_xZrO_3$) where $x$=0.05, 0.1, 0.2, 0.25 mole were synthesized by the conventional solid state method and sintering procedures. Experimental XRD-measurements indicated that Thorium dopant can substitute successfully on the A-sites of lead zirconate without damaging the main crystal structure which found to be orthorhombic phase with *Cmmm* space group. Scannin electron microscopy indicated that the average grain size of thorium-doped-lead zirconate ranged in between 0.35 and 1.43 µm. A Visualized studies were made to confirm success of thorium doping in the A-sites of perovskite structure. Theoretical investigations done were concerned by matching and comparison of bond distances ,torsions on angles of investigated compound to clarify success of thorium doping on the perovskite structure. Thermal analyses TGA&DTA were also attempted and incorporated to clarify the effect of thorium doping on thermal behavior of doped perovskite. Furthermore the effect of low concentration thorium dopings on the magnetic order, grain size and vibrational modes frequencies of infrared-spectra were studied.

Corresponding Authors
Tel; +9660503252190
E-Mail: ksabawy@yahoo.com
[a] Chemistry Department,Faculty of Science,Tanta University-31725-Tanta-Egypt
[b] Chemistry Department-Faculty of Science-Taif University-Taif City –888-Alhawyah-Saudi Arabia

## Introduction

Perovskite antiferroelectric (AFE) materials usually display larger field-induced strains, higher energy storage density, considerable pyroelectric coefficient and giant electro-caloric effect due to its unique electric-field-induced phase transformation characteristics between ferroelectric (FE) and AFE. Hence, AFE materials have potential applications in micro-actuators, IR-detectors, digital memories, high energy storage capacitors and cooling devices. Pure $PbZrO_3$ (PZ) with a Curie point of 230 C is the most stable AFE material at room temperature.[5] PZ-based materials in bulk and film forms are also the most extensively investigated AFE materials at present. There are a lot of reports on PZ-based AFE materials, such as: (Pb,La)$ZrO_3$ (PLZ), (Pb,Ba)$ZrO_3$ (PBZ), (Pb,Sr)$TiO_3$ (PST), $(Pb_{0.97}La_{0.02})(Zr,Ti,Sn)O_3$ (PLZST) and $(Pb_{0.99}Nb_{0.02})(Zr,Ti,Sn)O_3$ (PNZST), and so on.[6-14] Most of the compounds with the general formula $ABO_3$ have the perovskite structure[15] in which "A" may be a mono-, di-, or tri-valent cation and "B" may be a penta-, tetra-,or tri-valent cation.[16]. Solid solutions of lead zirconate-titanate ($PbZrO_3$ – $PbTiO_3$ system) attract the attention of researchers and developers in various fields of science and technology because of their potential applications in memories, microwave tunable capacitors, micro-electromechanical systems (MEMS), pyroelectric sensors and electro-optical switches[17-27] It is also reported that the antiferroelectric (AFE) to ferroelectric transition leads to significant energy storage for a dc field. This feature of $PbZrO_3$ makes it a specific material for energy storage applications.[28]

Preparation of lead zirconate or (PZ) by conventional processes requires the use of high temperatures at which PbO volatility becomes significant. It is reported that the full development of pure $PbZrO_3$ phase occurs after sintering at temperatures above 1200c° for at least 2h in controlled PbO atmospheres.[29-32] PZ powders can also be prepared by wet-chemistry based process routes, which include chemical co-precipitation[33,34], micro-emulsion[35] and sol-gel technique.[29]

Matthes et al.[35] prepared PZT thin films by the deposition a sol slurry, this method consists of a PZT-sol on acetic acid basis and PZT powder .Kong et al.[36] prepared PZ by a high-energy ball milling process using oxides as starting materials.

Bharadwaja et al.[37] studied the X-ray diffraction (XRD) for lead zirconate and La-doped lead zirconate thin films and reported that pure lead zirconate thin films showed a pseudo-cubic (110) orientation, whereas all the La-modified films showed a pseudo-cubic (111) orientation. The XRD analysis for lead lanthanum zirconate titanate (PLZT) thin films has been studied[38] and showed that the PLZT thin films are polycrystalline and the lattice parameter *a* decrease slightly with increasing La concentrations.

Boutarfaia[39] studied XRD, differential thermal analysis (DTA) and thermal gravimetric analysis (TGA) for $x$$PbZrO_3$-(0.95-$x$)$PbTiO_3$-0.05$Pb(Fe_{1/5},Ni_{1/5},Sb_{3/5})O_3$, it was reported that, the endothermic peak observed at about 240 °C is due to $Pb_3O_4$ decomposition and a appreciable weight loss of 2.5% is found with TGA, and another endothermic

signal at 560 °C which is related to $Pb_3O_4$ final decomposition.

The scanning electron microscope (SEM) has been studied[33] for $PbZrO_3$ and showed the sub-micrometer and spherical nature of the $PbZrO_3$ powder.

Akimov[40] studied the IR spectra of lead zirconate- titanate with a rhombohedral and a tetragonal structures and it has been established that with increase in the content of lead titanate in solid solutions of lead zirconate-titanate with a tetragonal structure, the frequency of the ferroelectric-active mode shifts toward higher frequencies.

The essential goal of present studies are studying the effect of low concentration thorium doping tetra-valent dopant on the A-site of perovskite on:

a) crystal structural of pure and Th-doped lead zirconate tetragonal- orthorhombic phases .

b) micro-structural feature and grain size of Th-doped samples ( $Pb_{1-x}Th_xZrO_3$ ).

c) magnetic order and thermal behavior of Th-doped-samples .

d) spectroscopic IR-absorption spectral frequencies of Th-doped samples .

## Experimental

### Samples Preparation

The pure lead zirconate ($PbZrO_3$) and thorium-doped samples with general formula ($Pb_{1-x}Th_xZrO_3$) where x = 0.05,0.1,0.2,0.25 mole were synthesized by the conventional solid state method and sintering procedure using appropriate amounts of $PbCO_3$, zirconyl carbonate, $ZrOCO_3$ and $ThO_2$ each of having purity >99%. The mixtures were ground in an agate mortar for 1h. The finely ground powder were subject to heating at 800 C° for 20 hrs then reground and pressed into pellets under compressive strength 8 ton/$m^2$ having the pellet dimensions (thickness 0.2 cm & diameter 1.2 cm). Sintering was carried out at 850 C° for 48 hrs. Then the furnace is cooled down slowly to room temperature. 10% more off-stoichiometric $Pb_3O_4$ were used in order to compensate lead deficient due to its sublimation during sintering process.

*X-Ray diffraction (XRD)*

The X-ray diffraction measurements (XRD) were carried out at room temperature on the fine ground powders of pure lead zirconate ( $PbZrO_3$ ) and thorium-doped samples with general formula ($Pb_{1-x}Th_xZrO_3$) where x = 0.05, 0.1, 0.2, 0.25 mole in the range ($2\theta$ =10-90°) using Cu-K$\alpha$ radiation source and a computerized [Steo-Germany] X-ray diffracto-meter with two theta ($2\theta$) scan technique. A visualized studies of crystal structure were made by using Diamond Molecular Structure version 3.2 package, Germany and Mercury 2.3-BUILD RC4-UK . A visualization study made is concerned by matching and comparison of experimental and theoretical data of atomic positions, bond distances, oxidation states and bond torsion on the crystal structure formed . Some of these data can be obtained free of charge from The Cambridge Crystallographic Data Centre via www.ccdc.cam.ac.uk/data_request/cif, or by emailing data request @ccdc.cam.ac.uk, or by contacting ICSD-Fiz-Karlsruhe-Germany .

*Scanning Electron – Microscope (SEM):*

Scanning electron microscope (SEM) measurements were carried out using small pieces of prepared samples on different sectors to estimate the actual molar ratios by using "TXA-840,JEOL-Japan" attached to XL30 apparatus with EDX unit, accelerant voltage 30kv, magnification 10x up to 500.000x and resolution 3 nm. The samples were coated with gold.

*Thermal Analyses Measurements*

The thermo-gravimetric analysis (TGA) and the differential thermal analysis (DTA) measurements were carried out on the green mixtures of the prepared samples using a computerized Shimadzu (Japan) TGA/DTA analyzer and $Al_2O_3$ as reference for DTA measurements. The heating rate was 3 degree/min and the cooling rate was 1degree/min.

*Solid Infrared Absorption Spectra Measurements*

The IR absorption spectra of the samples were recorded using "Perkin Elmer" Infrared Spectrophotometer, Germany in the range 200-1500 $cm^{-1}$ using spec. Pure KBr matrix.

*Magnetic Order Measurements*

The electron spin resonance spectra (ESR) were recorded at x-band frequencies on a "Bruker-Germany" ESR Spectrometer at room temperature at the National Research Center, Egypt. The magnetic field was swept from 0 to over 8 KG and the calibrated energy was 1 KG with a digital gaussmeter. Several selected samples were investigated.

## RESULTS AND DISCUSSION

### Phase Identification

Fig.1 displays the X-ray diffraction patterns of pure lead zirconate ($PbZrO_3$) and Th-doped $PbZrO_3$ ($Pb_{1-x}Th_xZrO_3$) perovskite where x=0.05, 0.1, 0.2, and 0.25 mole. Analysis of the corresponding $2\theta$ values and the inter-planar spacing *d* (Å) proved that, the compound mainly belongs to orthorhombic crystal structure with *Cmmm* space group.

The unit cell dimensions were calculated using the parameters of the most intense X-ray reflection peaks and were found to be *a*=11.8642 Å, *b* = 12.09 Å and *c* = 8.6345 Å for the pure $PbZrO_3$ . Even though PZ was first reported

to be tetragonal[41] at room temperature, single-crystal studies revealed the structure to be orthorhombic.[42] The present XRD patterns of PZ are in full agreement with results reported by Fang et al.[34] and Kong et al.[36]

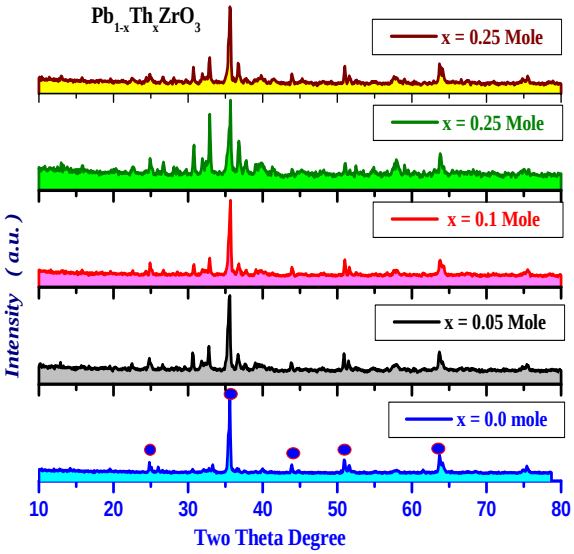


**Figure 1.** Room temperature XRD-patterns: (a) $PbZrO_3$; (b) $Pb_{0.95}Th_{0.05}ZrO_3$; (c) $Pb_{0.9}Th_{0.1}ZrO_3$; (d) $Pb_{0.8}Th_{0.2}ZrO_3$; (e) $Pb_{0.75}Th_{0.25}ZrO_3$.

It was observed that *c*-axis exhibits slight length compression by increasing Th-content as shown in Fig.(1a) due to ionic radius of Th-ion ($Th^{4+}$=102 pm) which is smaller than that of Pb-ion such that, $Pb^{2+}$=120pm.

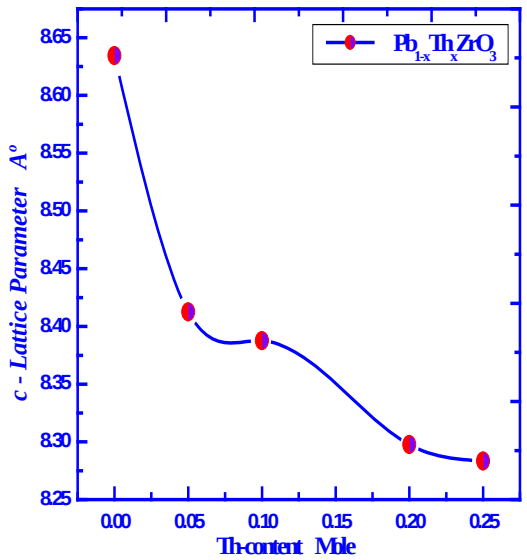


**Figure 1a.** Variation of c-axis lattice parameter as function of thorium content .

Although most of the compounds with the general formula $ABO_3$ have the perovskite structure[15] in which "A" may be a mono-, di-, or trivalent cation and "B" may be a penta-, tetra-, or trivalent cation.[16] In the present investigation tetravalent thorium successes within the investigated range to replace lead ($Pb^{+m}$, where $2 < m < 4$) in the main crystalline structure of perovskite without damaging the original orthorhombic perovskite crystal.

**Structure Visualization**

To confirm the success of tetravalent thorium to replace lead on the lattice structure of perovskite (A-site) a visualized crystal structure investigations were made depending upon single crystal data of lead zirconate supplied from ICSD-data bank Karlsruhe-Germany code number ICSD# 86443[43] see Figs.2a,b .

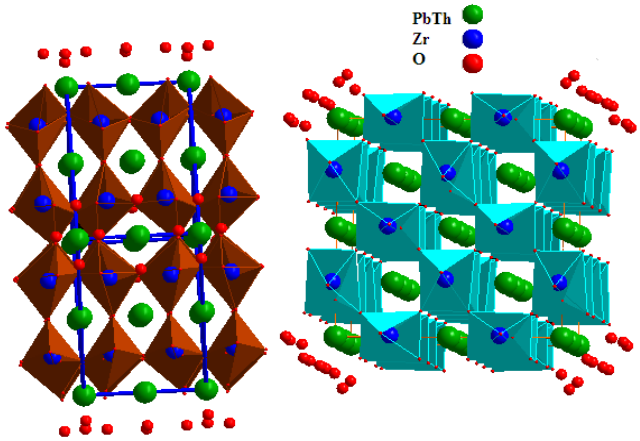


**Figure 2a** 2D-frame net and side view of thorium-doped lead zirconate perovskite unit cell.

Fig.2a shows 2D-frame net structure of orthorhombic perovskite structure displaying the different geometries of (Pb/Th)=A-sites and Zr=B-sites beside displaying the different orientation of polyhedron-zirconate inside unit cell of perovskite structure as clear in Fig.2b.

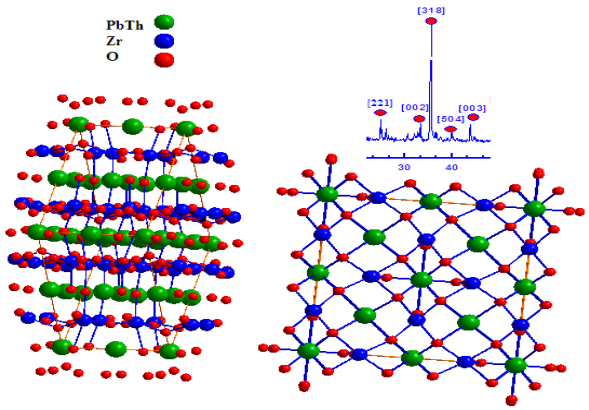


**Figure 2b.** Unit cell of Th-doped zirconate displaying $ZrO_6$-polyhedral units

Fig.2c shows the indexed XRD-profile for pure lead zirconate with $I_o$ index = {318} which lies at $2\theta \sim 35.8$ . The most intense reflection peaks ( fingerprint ) of lead zirconate were represented by red circles as clear in Fig.$2_c$ .It was noticeable that at two theta ($2\theta$) ~ 51.4 there is doublet

**Table 1.** Selected bond distances and angles inside crystal lattice of Th-doped-lead zirconate .

| $Atom_1$ | $Atom_2$ | Sym. Oper.1 | $d_{1-2}$ | $Atom_3$ | Sym. Opr.2 | $d_{1-3}$ | Angle 213^ |
|---|---|---|---|---|---|---|---|
| Pb1\|Th1 | O1 | -x, -y, z | 1.9461 | O1 | x, y, z | 1.9461 | 180.000 |
| | O1 | -x, -y, z | 1.9461 | O5 | x, y, z | 2.1570 | 124.046 |
| | O5 | x, y, z | 2.1570 | O5 | x, -y, -z | 2.1570 | 111.908 |
| | O5 | x, y, z | 2.1570 | O5 | -x, y, -z | 2.1570 | 97.369 |
| Pb2\|Th2 | O6 | 0.5-x, 0.5-y, z | 2.4102 | O6 | 0.5+x, 0.5-y, -z | 2.4102 | 118.991 |
| | O6 | 0.5-x, 0.5-y, z | 2.4102 | O6 | 0.5-x, -0.5+y, -z | 2.4102 | 115.995 |
| | O6 | 0.5-x, 0.5-y, z | 2.4102 | O6 | 0.5-x, 0.5-y, -z | 2.4102 | 85.581 |
| | O6 | 0.5-x, 0.5-y, z | 2.4102 | O6 | 0.5+x, -0.5+y, -z | 2.4102 | 180.000 |
| Pb4\|Th4 | O6 | 0.5-x, -0.5+y, 1-z | 2.2861 | O6 | 0.5+x, -0.5+y, 1-z | 2.2861 | 67.935 |
| | O6 | 0.5-x, -0.5+y, 1-z | 2.2861 | O6 | 0.5+x, 0.5-y, 1-z | 2.2861 | 101.369 |
| | O6 | 0.5-x, -0.5+y, 1-z | 2.2861 | O6 | 0.5-x, 0.5-y, 1-z | 2.2861 | 64.710 |
| | O6 | 0.5-x, -0.5+y, 1-z | 2.2861 | O6 | 0.5-x, 0.5-y, z | 2.2861 | 112.065 |
| Pb5\|Th5 | O5 | 0.5-x, 0.5-y, z | 2.4836 | O5 | 0.5-x, 0.5-y, -z | 2.4836 | 51.553 |
| | O5 | 0.5-x, 0.5-y, z | 2.4836 | O5 | x, y, -z | 2.4836 | 180.000 |
| | O5 | 0.5-x, 0.5-y, z | 2.4836 | O5 | x, y, z | 2.4836 | 128.447 |
| | O5 | x, y, -z | 2.4836 | O5 | x, y, z | 2.4836 | 51.553 |

**Table 2.** Selected bond distances and angles inside crystal lattice of Th-doped-lead zirconate

| $Atom_1$ | $Atom_2$ | Sym. Oper.1 | $d_{1-2}$ | $Atom_3$ | Sym. Opr.2 | $d_{1-3}$ | Angle 213^ |
|---|---|---|---|---|---|---|---|
| Zr1 | O3 | x, y, z | 1.5066 | O1 | x, y, z | 1.8329 | 140.289 |
| | O1 | x, y, z | 1.8329 | O5 | x, y, z | 2.2210 | 56.003 |
| | O5 | x, -y, z | 2.2210 | O5 | x, y, z | 2.2210 | 79.761 |
| Zr2 | O2 | x, y, z | 1.5781 | O4 | x, y, z | 1.6000 | 153.370 |
| | O4 | x, y, z | 1.6000 | O5 | -x, y, z | 2.0079 | 94.843 |
| | O5 | -x, y, z | 2.0079 | O5 | x, y, z | 2.0079 | 73.944 |
| | O6 | -x, y, z | 2.0294 | O6 | x, y, z | 2.0294 | 78.010 |
| O1 | Zr1 | x, y, z | 1.8329 | Zr1 | x, -y, -z | 1.8329 | 122.436 |
| | O5 | x, y, z | 1.9338 | O5 | x, -y, -z | 1.9338 | 135.099 |
| O2 | Zr2 | -x, y, -z | 1.5781 | Zr2 | x, y, z | 1.5781 | 145.486 |
| | O5 | -x, y, -z | 1.9460 | O5 | x, y, -z | 1.9460 | 76.71 |
| O3 | Zr1 | x, -y, 1-z | 1.5066 | Zr1 | x, y, z | 1.5066 | 158.142 |
| O4 | Zr2 | -x, y, 1-z | 1.6000 | Zr2 | x, y, z | 1.6000 | 161.253 |
| O5 | O1 | x, y, z | 1.9338 | O2 | x, y, z | 1.9460 | 109.573 |
| | O2 | x, y, z | 1.9460 | Pb1\|Th1 | x, y, z | 2.1570 | 74.958 |
| | Zr2 | x, y, z | 2.0079 | Pb1\|Th1 | x, y, z | 2.1570 | 106.153 |
| | Pb1\|Th1 | x, y, z | 2.1570 | O5 | x, y, -z | 2.1600 | 59.954 |
| | Zr1 | x, y, z | 2.2210 | O5 | -x, y, z | 2.4152 | 136.875 |
| O6 | Zr2 | x, y, z | 2.0294 | Zr10.5 | -x, 0.5-y, z | 2.0946 | 164.190 |
| | Zr1 | 0.5-x, 0.5-y, z | 2.0946 | Pb4\|Th4 | -0.5+x, 0.5+y, z | 2.2861 | 98.639 |
| | Pb4\|Th4 | -0.5+x, 0.5+y,z | 2.2861 | Pb2\|Th2 | -0.5+x, 0.5+y, z | 2.4102 | 82.106 |
| | Pb2\|Th2 | -0.5+x, 0.5+y,z | 2.4102 | O6 | x, 1-y, z | 2.4468 | 59.495 |

peak characteristics for lead zirconate perovskite structure indexed by {318), the same doublet peak was observed also nearly in the same location in the visualized theoretical patterns constructed for thorium-doped zirconate as clear in Fig.2d which confirm that thorium can substitute successfully on A-sites of perovskite structure without destroying the original orthorhombic phase .

The comparison between theoretical pattern Fig.2d and the experimental XRD-profile of thorium-doped lead zirconate Fig.2c one may conclude that there are moderate to strong fitting between the both profiles which confirm success of thorium doping within investigating range (0.05-0.25 mole).

Tables.1 and 2 show some selected bond distances and angles inside unit cell of Th-doped –perovskite zirconate.

From Table 1 one can observe that there are five types of A-sites (Pb/Th) according to the data found with five different environment namely ; $Pb_1/Th_1$ ,$Pb_2/Th_2$, $Pb_3/Th_3$, $Pb_4/Th_4$ and $Pb_5/Th_5$, it was noticed that the bond distances estimated for type one of A-sites ($Pb_1/Th_1$) were recorded and exhibited minimum bond distances with neighbouring oxygen atoms as clear in Table.1. Since $Pb_1/Th_1$-$O_1$ =1.94

Å and $Pb_1/Th_1$-$O_5$ = 2.157Å, while maximum bond distance were recorded for $Pb_5/Th_5$-$O_5$ which found to be equal 2.4836 Å.

These results are in full agreement with Coker et al.[44] who reported that the average bond distances recorded inside the crystal lattice of lead zirconate were found 2.47 Å for lead type 1 $Pb_1$-O and 2.58Å for lead type 2 $Pb_2$-O respectively .

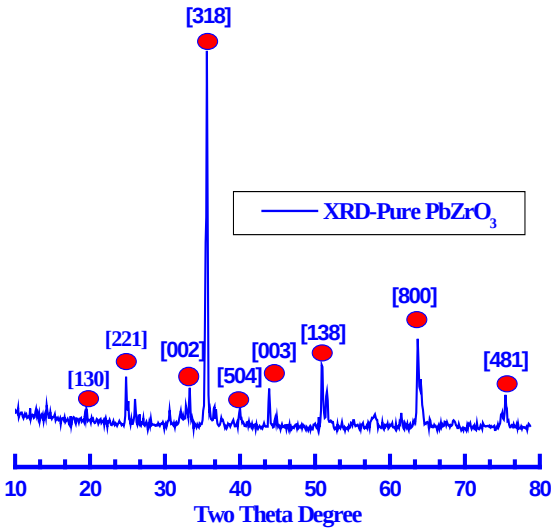


**Figure 2c.** Indexed XRD-profile recorded for pure lead zirconate

The analysis of bond distances and angles inside unit cell of Th-doped-lead zirconate indicated that there are two types of zirconium environment nominated as $Zr_1$ and $Zr_2$ as described in Table 2. This is beside six types of oxygen environment symbolized as $O_1$, $O_2$, $O_3$, $O_4$, $O_5$ and $O_6$ respectively .

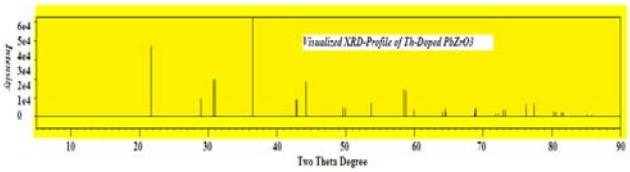


**Figure 2d.** Visualized XRD-profile recorded for Th-doped lead zirconate

It was noticed that the bond distances between Zr-O recorded minimum for ($Zr_1$-$O_3$ =1.50 Å) and maximum one is for $Zr_1$-$O_5$ with bond length = 2.22 Å while the other type was found to be 1.57 is for $Zr_2$-$O_2$ and 2.029 for $Zr_2$-$O_6$ respectively.

From Table 2 it was observed also that there are six types of oxygen symbolized as $O_1$, $O_2$, $O_3$, $O_4$, $O_5$ and $O_6$ are found inside lattice recorded bond distance values 1.83, 1.57, 1.5, 1.6, 2.007 and 2.029 Å for $O_1$-$Zr_1$, $O_2$-$Zr_2$, $O_3$-$Zr_1$ , $O_4$-$Zr_2$, $O_5$-$Zr_2$ and $O_6$-$Zr_2$ Å respectively .

These results are compatible with average bond distances recorded for the two types of zirconium ($Zr_1$and $Zr_2$ )-Oxygen inside crystal lattice was reported[44] for lead zirconate with small differences due to thorium doping effect. The authors[44] recorded the following bond distances for the two different types of zirconium $Zr_1$-$O_2$ = 2.111 Å ,$Zr_1$-$O_1$= 2.098 Å ,$Zr_2$-$O_3$= 2.162 Å ,$Zr_2$-$O_4$ = 2.140 Å and $Zr_2$-$O_5$ = 2.044 Å respectively .

The analysis of visualized structure concerning by XRD-pattern, bond distances, angles, torsion and lattice volume confirmed that stability of doped-lead zirconate lattice is relatively high specially there is no violation in most data recorded for thorium-doped- lead zirconate and consequently reflects success of thorium doping in the investigated range ($x$=0.05-0.25 mole).

**SEM Measurements**

Fig. 3 shows the SEM-micrographs for pure and Th-doped $PbZrO_3$ with (x=0.05, 0.1, 0.2 and 0.25) applied on the ground powders that prepared by solid state route (SSR) and it shows the sub-micrometer and spherical nature of the $PbZrO_3$ powder. The average grain size was calculated and found in between 0.35 and 1.43 µm.

These results are in agreement with results reported by Rao et al.[32] and Fang et al.[34] in which the conventionally $PbZrO_3$ powder is covering the size range from 0.2 to 1.3 µm. From Fig.3a-e it is so difficult to observe inhomogeneitiy within the micrograph due to that the powders used are very fine and the particle size estimated is too small. It was noticeable that the surfaces of all samples have bubbling nature as clear in Figs.$3_{a\text{-}e}$ due to precursor of the lead zirconate contains both of zirconium and lead as carbonates .And as result of raising temperature carbonates decomposes converting into $CO_2$ which make as bubbling agent .

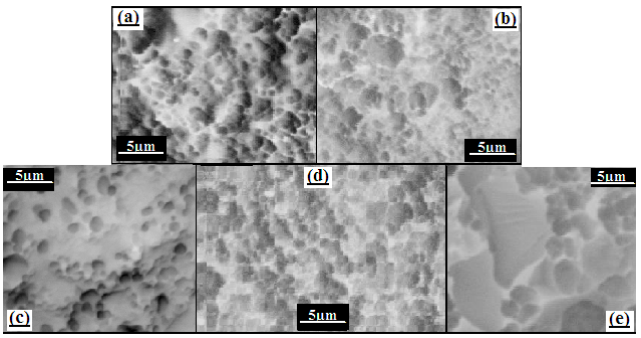


**Figure 3.** SE-micrographs captured for (a) $PbZrO_3$; (b) $Pb_{0.95}Th_{0.05}ZrO_3$; (c) $Pb_{0.9}Th_{0.1}ZrO_3$; (d) $Pb_{0.8}Th_{0.2}ZrO_3$; (e) $Pb_{0.75}Th_{0.25}ZrO_3$.

The grain size for Th-doped $PbZrO_3$ was calculated according to Scherrer's formula:

$$B=0.87\lambda/D\cos\theta \quad \text{.....(1)}$$

where *D* is the crystalline grain size in nm, θ is the half of the diffraction angle in degree, λ is the wavelength of X-ray source (Cu-$K_\alpha$) in nm, and B is the degree of widening of diffraction peak which is equal to the difference of full width at half maximum (FWHM) of the peak at the same diffraction angle between the measured sample and standard one. From SEM-maping, the estimated average grain size was found to be in between 0.35 and 1.43 µm which is relatively large in comparison with that calculated applying Scherrer's formula for pure 123-phase ($D \sim 0.39$ µm). This indicates that, the actual grain size in the material bulk is smaller than that detected on the surface morphology.

Furthermore, in our EDX (energy disperse X-ray) analysis, $Th^{4+}$ was detected qualitatively with good approximate to the actual molar ratio but not observed at $PbZrO_3$ grain boundaries which confirm that, thorium (IV) has diffused regularly into material bulk Th-doped $PbZrO_3$ perovskite-phase and induces in the crystalline structure of $PbZrO_3$ perovskite through solid state reaction.

**Infrared Absorption Spectra Measurements**

Fig. 4 shows the solid Infrared spectra for pure and Th-doped $PbZrO_3$ powders, the spectra for pure $PbZrO_3$ displays some characteristics bands at 417,551,750 and 812 $cm^{-1}$ which have been assigned generally to $ZrO_3$ torsions and those at 551 and 750 $cm^{1-}$ are due to Zr-O stretching and the other weak and much weaker bands appearing at higher wavenumbers result from the valent oscillation of metal-O bands.[45]

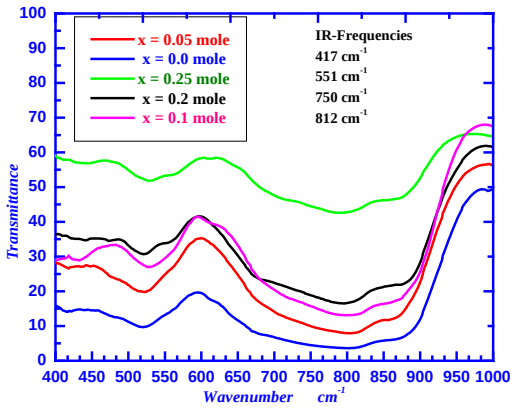


**Figure 4.** Infrared absorption spectra (a) $PbZrO_3$; (b) $Pb_{0.95}Th_{0.05}ZrO_3$; (c) $Pb_{0.9}Th_{0.1}ZrO_3$; (d) $Pb_{0.8}Th_{0.2}ZrO_3$; (e) $Pb_{0.75}Th_{0.25}ZrO_3$

For Th-doped lead zirconate , absorption bands of FT-IR spectrum are related to the lattice vibration of $BO_6$ (B¼Zr) octahedron groups,[46-48] a strong and broad band within 700–400 $cm^{-1}$ indicated the presence of $ZrO_6$ oxygen-octahedral groups, absorption bands within 700–500 and 500–400 $cm^{-1}$ represented the stretching frequencies of $ZrO_6$ oxygen-octahedral groups. Therefore, these observed infrared spectrum bands were all the characteristic bands of the perovskite PZ structure, further proving that the formation of perovskite-phase PZ via the solid state chemical reactions in heterogeneous multi-material powder mixtures.[49] It was noticed that some of Zr–O bond length decreased, so the bond force constant of *K* increased, and vibration frequency of $ZrO_6$ oxygen-octahedral groups got bigger, thus the strongest adsorption band shifted to a higher wave number for synthesized powders.

Based on these observations, it could be inferred due to which the crystal structure of synthesized powders is distorted. Thus the powders have high activity, which can reduce sintering temperature.

**Electron Spin Resonance (ESR) Measurements**

Fig. 5 displays the electron-spin resonance (ESR) spectra recorded for pure and Th-doped $PbZrO_3$ powders with ( x= 0.0 ,0.05 ,0.1 and 0.2 mole ), the *g*-values parallel and perpendicular to the symmetry axis and the effective *g*-values which nominated as ($g_{iso}$) are calculated as shown in Table 3.

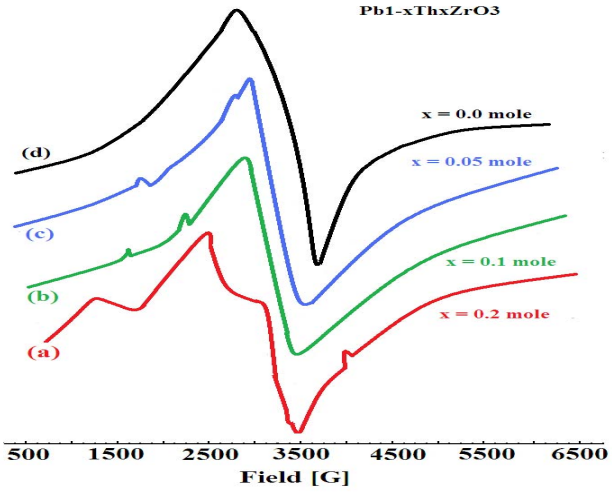


**Figure 5.** ESR-signals recorded for pure and selected thorium doped zirconates; (a) $PbZrO_3$; (b) $Pb_{0.95}Th_{0.05}ZrO_3$; (c) $Pb_{0.9}Th_{0.1}ZrO_3$; (d) $Pb_{0.8}Th_{0.2}ZrO_3$.

It was obvious to observe that the values of ($g_{iso}$) is inversely proportional to the dopant ratio, recording minimum value ($g_{iso}$) =2.13 for highest dopant content Th=0.2 mole.

**Table 3.**The effective g-values ($g_{iso}$) of some prepared samples of Th-doped $PbZrO_3$.

| **Material** | **$g_{iso}$ values** |
|---|---|
| $PbZrO_3$ | 2.31 |
| $Pb_{0.9}Th_{0.05}ZrO_3$ | 2.28 |
| $Pb_{0.8}Th_{0.1}ZrO_3$ | 2.24 |
| $Pb_{0.75}Th_{0.25}ZrO_3$ | 2.13 |

This decrease in the paramagnetic content is due to that thorium dopant has tetra-valent oxidation state which means the outer shell is vacant since the electronic configuration of

thorium is [Rn] $6d^27s^2$ , for tetra-valent thorium ($Th^{4+}$)=[Rn] $6d^07s^0$ and consequently the diamagnetic character is increased remarkably as Th-doping ratio increased .

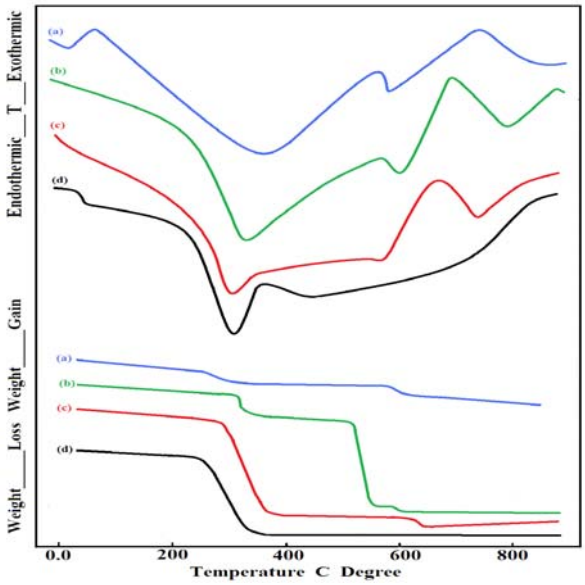


**Figure 6.** TGA/DTA curves: (a) $PbZrO_3$; (b) $Pb_{0.95}Th_{0.05}ZrO_3$; (c) $Pb_{0.9}Th_{0.1}ZrO_3$; (d) $Pb_{0.8}Th_{0.2}ZrO_3$.

Analysis of its ESR spectra indicates that $Th^{4+}$ substitution occurs at the $Pb^{n+}$ at many different ESR-distinguishable locations. All factors, namely could be for the $Pb^{4+}$>$Pb^{2+}$, $Pb^{3+}$>$Pb^{2+}$ or $Pb^{4+}$>$Pb^{2+}$ $Pb^{4+}$>$Pb^{3+}$ conversions which are responsible for the large microstrains and the deterioration of crystalline structure is observed in these ceramics, which seemed to play a crucial role for reading large piezoelectric anisotropy within thorium-doped perovskite system. Although $Pb^{3+}$ is not real valency for lead but it is really observed in visualised calculation as average oxidation state for lead ($Pb^{4+}$ and $Pb^{2+}$) inside crystal lattice .

These results are partially in agreement with the results of Rosales et al.[50] who investigated the effect of Eu-and Ti-doping on the ESR spectra of lead manganate perovskite structure.

#### Thermal Analyses Measurements

The TGA and DTA analyses were carried out on the green mixtures of pure and Th-doped $PbZrO_3$ powders with (x=0.0, 0.05, 0.1 and 0.2 mole ) symbolized as a, b, c and d respectively in Fig. 6.

From TGA/DTA curves Fig.6 the TGA analysis can be divided into four steps. The first step occupies the region from room temperature up to 230°C for which the weight loss occurred is attributing to the humidity of samples and partial decomposition of both of $ZrOCO_3$ and $PbCO_3$ The second region lies between 240~390 °C at which lead carbonate decomposed moderately into PbO and $CO_2$.[39]. The third region of temperature ranging from 390-680 °C at which the weight loss occurred attributing to the onset of the crystallization process and partial volatilization of lead oxide.[39,51] The last region is between 680~800 °C for complete decomposition of both of $Zr(CO_3)_2$ and $PbCO_3$ into metal oxide accompanied with solid state reaction of solid metal oxide (Pb-oxide,$ThO_2$ and $ZrO_2$) .

The same trend was observed[52-54] for the endothermic peak, which always observed at approximated range of ~ 780-820 °C which refers to the phase formation and this range could be shifted up or down according to the system composition under investigations.

## Conclusions

The conclusive remarks within this article can be summarized under the following points;

Tetravalent thorium got success in the investigated range to replace lead in the main crystalline structure of perovskite without damaging the original orthorhombic perovskite crystal.

The analysis of visualized structure determined by XRD-pattern, bond distances, angles, torsion and lattice volume confirmed that stability of doped-lead zirconate lattice is relatively high, specially there is no violation in most data recorded for thorium-doped- lead zirconate and consequently reflects success of thorium doping in the investigated range (x=0.05-0.25 mole )

The SEM measurements indicated that the average grain size of thorium-doped-lead zirconate ranged in between 0.35 and 1.43 μm.

Decreasing of paramagnetic content is due to the diamagnetic character is increased remarkably as Th-doping ratio increased .

## References

[1]Park, S. E. Markowski, K. Yoshikawa S. and Cross, L. E. *J. Am. Ceram. Soc.* **1997**, *80*, 407.

[2]Parui, J. and Krupanidhi, S. B., *J. Appl. Phys.* 100 (2006), pp. 044102.

[3]Xu, Z. K. Zhai, J. W. and Chan, W. H., *Appl. Phys. Lett.* **2006**, *88*, 132908.

[4]Love, G. R. *J. Am. Ceram. Soc.* **1990**, *73* 323.

[5]Chattopadhyay, S., Ayyub, P., Palkar, V. R., Multani, M. S., Pai, S. P., Purandare S. C., Pinto, R., *J. Appl. Phys.* **1998**, *83*, 7808.

[6]Bharahwaja S. S. N. and Krupanidhi, S. B. *Thin Solid Films* **2003**, *423*, 88.

[7]Xu, B. M., Ye, Y. H. and Cross, L. E., *J. Appl. Phys.* **2000**, *87*, 2507.

[8]Zhai, J.W. Cheung, M.H. Xu Z.K. and Li, X. *Appl. Phys. Lett.* **2002**, *81*, 3621.

[9]Chen, H. W., Yang, C. R., Zhang, J. H., Pei, Y. F. and Zhao, Z. *J. Alloys Compd.* **2009**, *486*,. 615.

[10]Hao, X. H. and Zhai, J. W., *J. Cryst. Growth*, **2008,** *310*, 1137.

[11]Hao, X. H., Zhai, J. W. and Yao, X. *J. Cryst. Growth*, **2008**, *311*, 90.

[12]Kong, L. B., Ma, J., Zhu, W. and Tan, O. K., *J. Alloys Compd.*, **2001**, *322*, 290.

[13]Charoonsuk, P., Wirunchit, S., Muanghlua, R., Niemcharoen, S., Boonchom B. and Vittayakorn, N., *J. Alloys Compd.3,* (2010)pp.23-28 .

[14]Hao, X. H. Zhang, Z. Q. Zhou, J. An, S. L. and Zhai, J. W. *J. Alloys Compd.* **2010**, *501*, 358.

[15]Smoluchowski R. and Kurti N., *Solid State Physics*, vol.5: *Structure, Properties, &Preparation of Perovskite-Type Compounds*, Pergamon Press Inc., **1969**, 3-11.

[16]Wold A. and Dwigh, K., Solid State Chemistry, Chapman and Hall Inc., **1993**. p. 127, 136, 137.

[17]Scott, J. F. Araujo, C. A., *Science,* **1989**, *246*, 1400.

[18]Xu, Y. H. *Ferroelectric Materials and Their Applications*, North-Holland, Amsterdam, **1991**, 206.

[19]Watton, R. Manning, P., *Proc. SPIE 3436*, **1998**, 541.

[20]Wood, V. E. Bush, J. R., Ramamurthi, S. D. Swartz, S. L., *J. Appl.Phys.* **1992**, *71*, 4557.

[21]Preston, K. D., Haertling, G. H., *Appl. Phys. Lett*., **1992**, *60*, 2831.

[22]Liu, W. G., Ko, J. S., Zhu, W. G., *Infrared Phys. Technol.*, **2000**, *41*, 169.

[23]Dimos, D. Muller, C. H., Ann. Rev. Mater. Sci., **1998**, *28*, 397.

[24]Polla, D. L., *Microelectron. Eng.*, **1995**, *29*, 51.

[25]Nemirovsky, Y., Nemirovsky, A., Muralt, P., Setter, N., *Sensors Actuators,* **1996**, *A56*, 239.

[26]Heartling, G., *J. Am. Ceram. Soc*., **1999**, *82*, 797.

[27]Singh, K. *Ferroelectrics*, **1989**, *94*, 433.

[28]Lanagan, M. T., Kim, J. H., Jang, S. and Newnham, R. E., *J. Am. Ceram. Soc*., **1988**, *71*, 111.

[29]Wakino, K., Murata, M. and Tamura, H., *J. Am. Ceram. Soc*., **1986**, *69*, 34.

[30]Lawless, W. N., *Phys. Rev*., **1984**, *B30*, 6555.

[31]Ibrahim, D. M. and Henniek, H. W., *Trans. J. Br. Ceram. Soc*., **1981**, *80*, 18.

[32]Rao, Y. S., Sunandana C. S., J. Mater. Sci. Lett., 1992, 11, 595.

[33]Oren, E. E. Taspinar E. and Tas, A. C., *J. Am. Ceram. Soc.*, **1997**, *80*(10), 2714.

[34]Fang, J., Wang, J., Ng, S. M., Gan, L., Quek C. and Chew, C. H., *Mater. Lett.,* **1998,** *36*, 179.

[35]Matthes, B. Tomandl, G. and Werner, G., *J. Eur. Ceram. Soc.,* **1999***, 19(6-7)*, 1387

[36]Kong, L. B., Ma, J., Zhu, W. and Tan, O. K., *Mater. Lett*., **2001**, *49(2)*, 96.

[37]Bharadwaja, S. S. N., Krupanidhi, S. B., *Thin Solid Films* **2003**, *423*, 88.

[38]Hu, Z. G., Shi, F. W., Lin, T., Huang, Z. M., Wang, G. S., Wu, Y. N., Chu, J. H., Phys. Lett. A, **2004**, *230,* 478.

[39]Boutarfaia, A. *Ceram. Int.*, **2001**, *27*, 91.

[40]Akimov, A. I., Savchuk, G. K., and Akimova, T. M., *J. Appl. Spectr.*, **2003**, *70*, 4.

[41]Megaw, H. D., *Proc. Phys. Soc. London*., **1946**, *58*, 133.

[42]Sawaguchi, E., Maniwa, H. and Hoshino, S., *Phys. Rev*., **1951**, *53*, 1078.

[43]Fujishita, H., Shiozaki, Y., Achiwa, N., Sawaguchi, E., *J. Phys. Soc. Japan*, **1982**, *51*, 3583.

44Corker, D. L., Glazer, A. M., Kaminsky, W., Whatmore, R. W., Dec, J., Roleder, K., *Acta Cryst.* 1998, B54, 18.

[45]Rao, C. **Perovskites Ceramics** ,Academic Press, 1963, p. 356 .

[46]Ghasemifard, M., Hosseini, S. M., Zak A. and Khorrami, G. H., *Physica E* **2009**, *41*, 418.

[47]Chang, T., Huang, J. L. and Lin, H. P., *J. Alloys Compd.* **2006**, *414*, 224.

[48]Smitha, P., Pandey P. K. and Gajbhiye, N. S. *Mater. Chem. Phys.,* **2008, 109**, 500.

[49]Chen, F., Yang, S. Y., Wang, J. X., He, H. L. and Wang, G. C., *J. Inorg. Mater.* **2007,** *22*, 827.

[50]Ramírez-Rosales, D., Zamorano-Ulloa R., and Pérez-Martínez, O., Solid State Comm. **2001**, *118*,.371-376

51Pandey, D., Singh, A. K., Srivastava, P., Singh, A., Inbanathan, P., and Singh, G., *Physica* **1995**, *C241*, 279.

[52]Sekkina, M. M. A., Elsabawy, K. M., *Physica C* **2002**, *377,* 254.

[53]Sekkina, M. M. A., Elsabawy, K. M., *Mater. Science Eng.,* **2003,** *B103*, 71.

[54]Elsabawy, K. M., Kandyel, E. E. and Sekkina, M. M. A., *Current Appl. Phys.*, **2009**, *9*, 238.

Received: 30.09.2010.

Accepted: 16.10.2012.